Effects of silver loading in zinc oxide on the photodegradation of methyl orange and methylene blue

Alan German Acedo-Mendoza[a], Diana Vargas Hernández[b,*], Diana Gabriela Domínguez Talamantes[a], Enrique Rodríguez Castellón[c], Judith Celina Tánori Córdova[a]

[a]*Departamento de Investigación en Polímeros y Materiales, Universidad de Sonora, Blvd. Luis Encinas y Rosales S/N, 83000 Hermosillo, Sonora, México, Tel. +52 6622592161; emails: alan.gam@gmail.com (A.G. Acedo-Mendoza), dgdt.1103@gmail.com (D.G. Domínguez Talamantes), jtanori@unison.mx (J.C. Tánori Córdova)*
[b]*CONACYT-Universidad de Sonora, Universidad de Sonora, Blvd. Luis Encinas y Rosales S/N, 83000 Hermosillo, Sonora, México, Tel. +52 6622592161; email: dvargashe@conacyt.mx (D. Vargas Hernández)*
[c]*Departamento de Química Inorgánica, Cristalografía y Mineralogía, Facultad de Ciencias, Universidad de Málaga, Campus de Teatinos, 29071 Málaga, Spain, Tel. +34 952131873; email: castellon@uma.es (E. Rodríguez Castellón)*

Received 8 June 2019; Accepted 11 July 2020

ABSTRACT

Silver-supported zinc oxide catalysts were tested for the photodegradation of methyl orange (MO) and methylene blue (MB) dyes under UV irradiation at 25°C. These Ag/ZnO catalysts, which variable silver loadings (1, 2 and 3 wt.%) were prepared by impregnation and characterized by atomic absorption spectroscopy, N_2 adsorption–desorption, X-ray diffraction (XRD), transmission electron microscopy, diffuse reflectance spectroscopy, X-ray photoelectron spectroscopy (XPS), and Fourier-transform infrared spectroscopy. The XRD, high-resolution transmission electron microscopy and XPS results revealed that ZnO was wurtzite phase, and metallic silver (Ag^0) was the support in ZnO nanorods; the crystal sizes were 72 and 18.4 nm in ZnO and Ag^0, respectively. The experimental results showed that the xAg/ZnO catalysts were highly active in MO and MB degradation compared with the zinc oxide supports because of the presence of metallic silver, which acted as an electron trap, thus inhibiting the electron-hole recombination. The 2Ag/ZnO catalyst exhibited greater degradation activity in both dyes, reaching 100% degradation after 30 and 90 min in MB and MO, respectively, because of the greater dispersion of the silver and the higher concentration of hydroxyl groups on the surface compared with the other catalysts. The effects of different scavengers of the main species involved, such as hydroxyl radicals, superoxide anions radicals and positive holes, which were studied to determine the photodegradation mechanisms of the dyes on these systems. The superoxide radical was the main reactive species during the photocatalytic degradation of MB and MO. Moreover, 2Ag/ZnO catalyst exhibited excellent photocatalytic stability and activity after five cycles.

Keywords: Photocatalysis; Methyl orange; Methylene blue; Silver; Zinc oxide

1. Introduction

The most common contaminants in wastewater are dyes derived from manufacturing industries as dyestuffs, textiles, paper, food, cosmetics, leathers and plastics [1]. These dyes in wastewater, even at very low concentrations, can potentially harmful to human health [2]. Organic dye molecules usually possess one or more benzene rings, which resist degradation by conventional biological and chemical methods [3,4].

* Corresponding author.

The technologies implemented to eliminate dyes in water are classified into two groups: one includes the separation of contaminant by adsorption, ion exchange, biological, precipitation [3–6]. Nevertheless, these methods are not destructive, and they concentrate or change the organic pollutions from the aqueous phase to a solid phase. Thus, additional costs are required to treat secondary pollutants and regeneration of the used adsorbent [7]. The second group includes the degradation the contaminants, by advanced oxidation processes based on the generation of oxidizing chemical species such as hydroxyl radicals ($^{\bullet}$OH) and superoxide radicals ($O_2^{\bullet-}$), with UV irradiation, which led to their almost complete mineralization them CO_2 and water [8–10]. In a typical heterogeneous photocatalytic process during the ultraviolet irradiation of a semiconductor in which the photogenerated electron-hole (e^-/h^+) pairs on the valence and conduction band reacted with dissolved oxygen and hydroxyl ion to form $O_2^{\bullet-}$ and $^{\bullet}$OH radicals, respectively, these radicals act as strong oxidizing agents for dye degradation because rapid oxidation was achieved at parts per billion (ppb) levels [11]. In recent years, semiconductor mediated photocatalysis has attracted interest because of its potential to destroy a wide range of organic and inorganic pollutants under ambient conditions without the production of harmful products [12]. The application of ZnO as a photocatalyst in the degradation of methylene blue (MB) and methyl orange (MO) dyes has attracted much attention because of its low cost, non-toxicity, high photosensitivity, wide bandgap and high chemical stability in association with the degradation of organic compounds [13–16]. Unfortunately, the recombination of e^-/h^+ pairs in the existing methods reduce its photocatalytic activity ability. So far, different methods of doping and supporting of semiconductors have been used to increase the photocatalytic activity of a single semiconductor [17]. In addition, catalytic improvement in the photodegradation dyes has been achieved by incorporating silver into ZnO; the presence of silver decreased the bandgap [18–20] and prevented electron-hole combination. This method has been shown to have remarkable catalytic potential, low cost, non-toxicity, high electrical, thermal conductivity and antibacterial activity [16,21]. Therefore, the combination of Ag and ZnO may offer an interesting solution. Several Ag and ZnO photocatalysts with different morphologies have been studied. Saravanan et al. [21] used ZnO/Ag in the degradation of MB and MO; Kuriakose et al. [22] used ZnO nanospindles with Ag nanoparticles in the degradation of MO; Zhang et al. [23] showed the photocatalytic performance of Ag/ZnO samples in the degradation of MB with visible light irradiation; Ansari et al. [24] used an Ag–ZnO nanocomposite in the photodecomposition of MO, MB and 4-nitrophenol with visible light; Lu et al. [25] used Ag on ZnO nanorods in the degradation of MO with a UV lamp.

In this present study, we studied prepared and characterized Ag/ZnO catalysts that are useful in the photodegradation of MB and MO under UV irradiation. When photodegradation occurred, silver loading was evaluated. The effects of different scavengers of main species involved, such as hydroxyl radicals, superoxide radicals anion and positive holes, were investigated to determine photodegradation mechanisms of the dyes. The correlation between structure and activity was established to elucidate the parameters governing the catalytic activity.

2. Methodology

2.1. Materials

The materials used in our experiments were zinc(II) oxide (ZnO, Merck, Kenilworth, New Jersey, United States of America), silver(I) nitrate ($AgNO_3$, Sigma-Aldrich, St. Louis, Missouri, United States of America), methyl orange ($C_{14}H_{14}N_3NaO_3S$, Sigma-Aldrich, St. Louis, Missouri, United States of America), methylene blue ($C_{16}H_{18}ClN_3S$, Sigma-Aldrich, St. Louis, Missouri, United States of America), coumarin ($C_9H_6O_3$, Sigma-Aldrich) and ammonium oxalate (($NH_4)_2C_2O_4$, Sigma-Aldrich, St. Louis, Missouri, United States of America).

2.2. Preparation of photocatalysts

Ag/ZnO catalysts were prepared by incipient wetness impregnation at different concentrations 0.09, 0.18 and 0.28 mol/L of $AgNO_3$ in 1 g of ZnO. After impregnation, the solids were dried at 40°C and calcined for 3 h at 500°C at 1°C/min. The catalysts were labeled as xAg/ZnO, where x refers to the Ag wt.% in the catalysts (x = 1, 2 and 3).

2.3. Samples characterization

The quantification of the silver content was determined by atomic absorption spectroscopy (AAS) using a Varian AA240FS (Palo Alto, California, United States of America). The surface area Brunauer–Emmett–Teller (S_{BET}), pore volume (V_p) and pore diameter (d_p) were obtained from N_2 adsorption–desorption isotherms of the photocatalyst at –196°C using a Micromeritics ASAP 2020 system (Micromeritics, Norcross, GA, USA). Prior to the N_2 adsorption–desorption, samples were degassed overnight at 500°C and 10^{-4} mbar. S_{BET} was calculated by the BET method [26]. Powder X-ray diffraction (XRD) analysis was performed on Bruker Model D8 Advance (Madison, Wisconsin, United States of America) using Mo Kαl (070932 Å) at 50 kV and 50 mA over a range of 10°–70° at a step time of 2.5 s and a step size of 0.01° to identify the crystalline phases and particle size. The crystalline sizes were calculated using the Scherrer method [27]. The surface morphology of the photocatalyst was examined by transmission electron microscopy (TEM) (JEOL 2010 F, Peabody, Massachusetts, United States of America). Diffuse reflectance spectroscopy (DRS) of the sample were obtained using a UV-vis spectrophotometer with an integrating sphere (Lambda 20, Perkin Elmer, Waltham, Massachusetts, United States of America). The bandgap energy (E_g) was determined as the intersection point between the energy axis and the line extrapolated from the linear portion of the absorption edge in a Kubelka-Munk function (F) plot against energy E (eV) [28]. X-ray photoelectron spectroscopy (XPS) were obtained using a Physical Electronics PHI 5700 spectrometer (Ulvac-Phi, Chanhassen, MN, USA) equipped with non-monochromatic Mg Kα radiation (500 W, 15 kV and 1,253.6 eV) and a multichannel detector. All spectra were measured in all cases using a constant pass energy mode at 29.35 eV, and a

diameter analysis area of 720 μm. The adventitious carbon (C 1s at 284.8 eV) was used as a reference. The A PHI ACCESS ESCA-V6.0F software package (Ulvac-Phi, Chanhassen, MN, USA) was used to collect and analyze the data. The signals were subtracted based on a Shirley-type background and fitted using Gaussian-Lorentzian curves to estimate the binding energies of the different element core levels. The surface hydroxyl groups were analyzed using Fourier-transform infrared spectroscopy (Perkin Elmer Frontier FTIR).

2.4. Photocatalytic activity

The photocatalytic degradations of MB and MO were studied under UV irradiation at 25°C. The reaction was carried out in a discontinuous mechanical stirring photoreactor at a reaction volume of 500 mL with a 400 W UV lamp. The lamp was placed inside a quartz container with two cabins: one contained the lamp and the other passed water into a recirculation channel for temperature control. Before irradiation, 150 mg of catalyst was added to the dye solution (0.45 L) and magnetically stirred in the dark for 30 min to reach adsorption equilibrium. Afterward, the UV lamp was switched on, and aliquots of the aqueous suspension were collected from the reactor every 5 min. The concentrations of MB and MO were determined by a UV-vis spectrophotometer (Agilent 8453, Santa Clara, California, United States of America) at 664 and 463 nm for MB and MO, respectively. The degradation efficiency was calculated as $(C_0 - C)/C_0$, where C_0 is the initial concentration and C is the temporal concentration after degradation.

2.5. Detection of hydroxyl and superoxide radicals and study of the positive hole

The concentration of hydroxyl radicals (•OH) generated by the formation of 7-hydroxycoumarin was traced by fluorescence spectroscopy (LS55, Perkin Elmer, 320 nm wavelength) [29]. For this purpose, a 2 mM coumarin solution was prepared, and 0.166 g of the photocatalysts to be studied were added. After the solution was irradiated with UV light for 30 min at 25°C, 5 mL aliquots were extracted at 5 min intervals. Finally, the fluorescence emission spectra of the irradiated solution were analyzed with ZnO as reference.

The absence of superoxide radicals ($O_2^{•-}$) was carried out with bubbled nitrogen in a solution containing 20 ppm solution of dye and 0.166 g of photocatalyst [30]. The solution was irradiated with UV light for 30 min at 25°C, and 5 mL aliquots were extracted at 5 min intervals for analysis by UV-vis spectrophotometry.

The evaluation of the capture of the positive hole using ammonium oxalate as the sacrificial agent was carried by bubbled nitrogen and an oxygen atmosphere [31,32] in a solution containing 20 ppm of dye, 4 mM of $(NH_4)_2C_2O_4$ and 0.166 g of the photocatalyst. The solution was irradiated with UV light for 30 min at 25°C, and 5 mL aliquots were extracted at 5 min intervals for analysis by UV-vis spectrophotometry.

2.6. Determination of nitrate and sulfate ions

Nitrate ions (NO_3^-) were analyzed by the cadmium reduction method using the NitraVer low range kit Hach (Loveland, Colorado, United States of America). Sulfate ions (SO_4^{2-}) were analyzed by the turbidimetric method, and the results showed that the SO_4^{2-} ions reacted with barium ions to form barium sulfate [33]. Turbidity was measured by spectrophotometry using a GENESYS 10S UV-Vis spectrometer (Thermo Scientific, Waltham, Massachusetts, United States of America).

3. Results and discussion

3.1. Characterization

The silver content of each catalyst, as determined by AAS, is shown in Table 1. The Ag content of the synthesized xAg/ZnO catalysts varied between 0.9 and 3.1 wt.%.

The N_2 adsorption–desorption isotherms at –196°C for ZnO and ZnO loaded with Ag are shown in Fig. 1. All samples are of typical IV isotherms according to the International Union of Pure and Applied Chemistry classification with H3 hysteresis [34]. In the present type of hysteresis loop, the pores of the catalysts were slit-shaped, which occurred between disordered aggregates of plate-like particles [34]. The form of the adsorption isotherm of ZnO was preserved in the silver-containing catalysts, after impregnation and subsequent calcination. The pore size was calculated by the Barrett–Joyner–Halenda method using the desorption branch of the isotherm which showed smaller mesopores [35]. Pore sizes of all catalysts ranged from 3–4 nm [23].

The textural parameters of the catalysts revealed that S_{BET} progressively decreased with metal loading (Table 1). These results can be due to the input limitation of ZnO by Ag nanoparticles and the blocking of the ZnO pore openings by silver deposition [12].

The XRD powder patterns of ZnO and Ag-containing ZnO samples are shown in Fig. 2. For ZnO, XRD peaks at $2\theta(°) = 31.8, 34.5, 47.5, 56.5, 62.9, 66.4, 67.9$ and 69.2 were

Table 1
Physicochemical characterisation of ZnO and xAg/ZnO catalysts

Sample	Ag loading (wt.%)	ZnO (nm)	Ag (nm)	S_{BET} (m²/g)	d_p (nm)	V_p (cm³/g)
ZnO	–	74.6	–	4.6	14.2	0.01
1Ag/ZnO	0.9	69.9	10.1	4.4	21.1	0.02
2Ag/ZnO	2.0	72.6	18.4	4.0	20.9	0.01
3Ag/ZnO	3.1	74.0	30.0	4.1	20.8	0.02
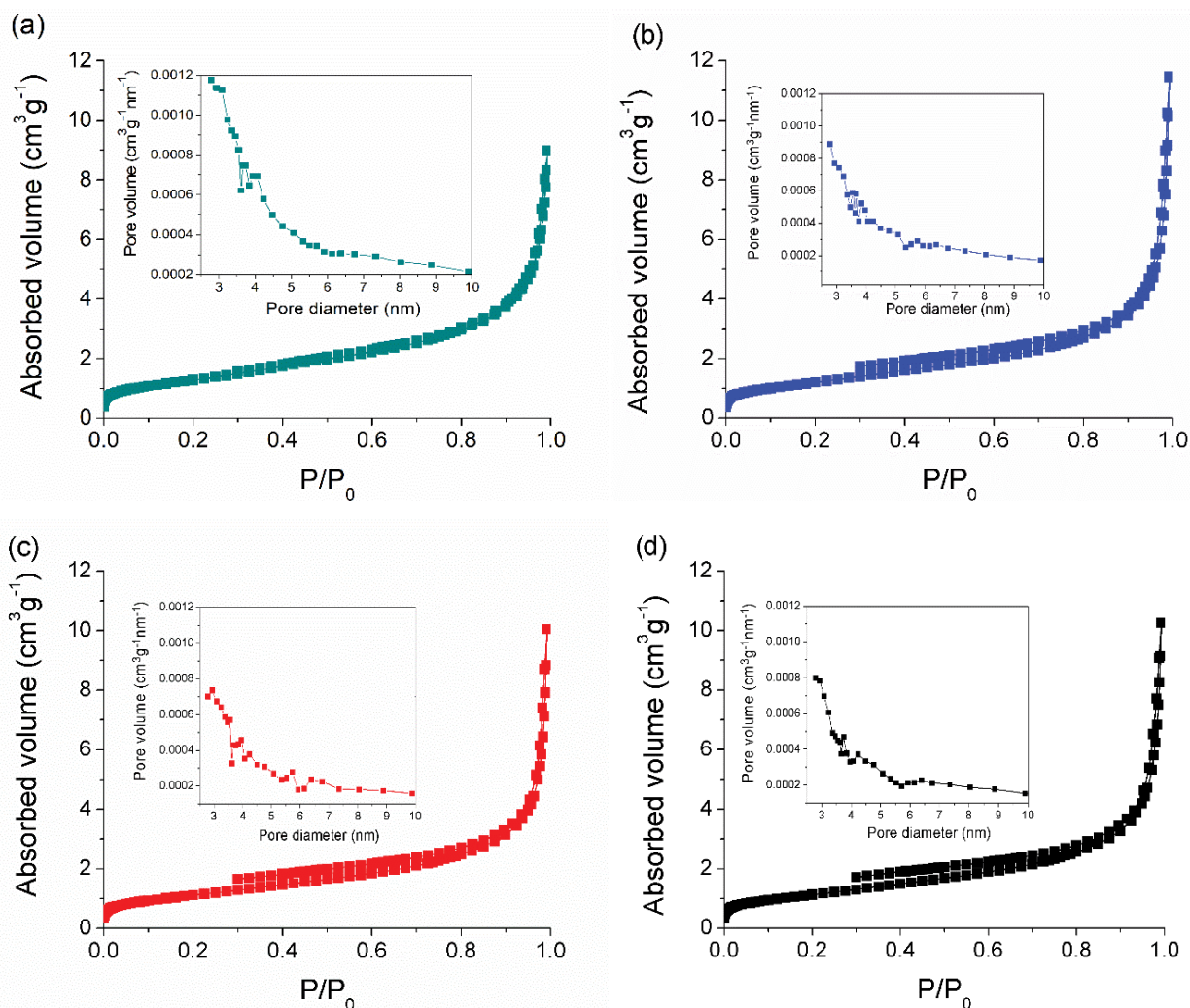
Fig. 1. N$_2$ adsorption–desorption isotherms at –196°C and pore size distributions of ZnO (a), 1Ag/ZnO (b), 2Ag/ZnO (c) and 3Ag/ZnO (d).
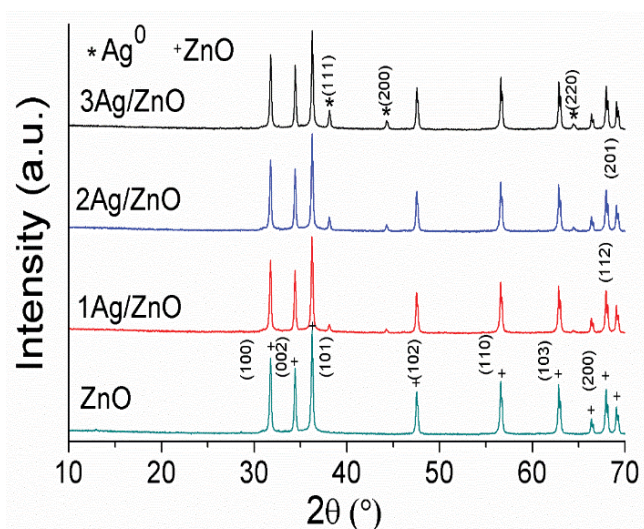
Fig. 2. XRD patterns of ZnO, 1Ag/ZnO, 2Ag/ZnO and 3Ag/ZnO.

observed, corresponding to (100), (002), (101), (102), (110), (103), (200), (112) and (201), crystallographic planes of the hexagonal wurtzite ZnO phase [JCPDS No. 01–080–0074], respectively [22,36]. Moreover, xAg/ZnO photocatalysts showed additional diffraction peaks at $2\theta(°)$ = 38.2, 45.0 and 63.0, which corresponded to (111), (200) and (220), crystallographic planes of the metallic silver (Ag^0) cubic phase [JCPDS No. 01–087–0597] [36]. The intensity of the Ag^0 peaks increased as the amount of silver in ZnO increased, which indicated that the size of the metal Ag particles increased. The particle sizes were calculated using the Scherrer formula [27]. The results of the calculations showed that the average crystal size of ZnO in Ag supported in the ZnO catalyst was constant at approximated 70 nm (Table 1). The increase in the sizes of silver crystallite in xAg/ZnO was greater at higher silver loadings, which was due to increases in the initial concentration of AgNO$_3$ and to changes in ionic radii of 1.26 and 0.74 Å for Ag and Zn^{2+}, respectively, [36,37]. The average crystallite size for Ag varied from 10 to 30 nm among the sample (Table 1).
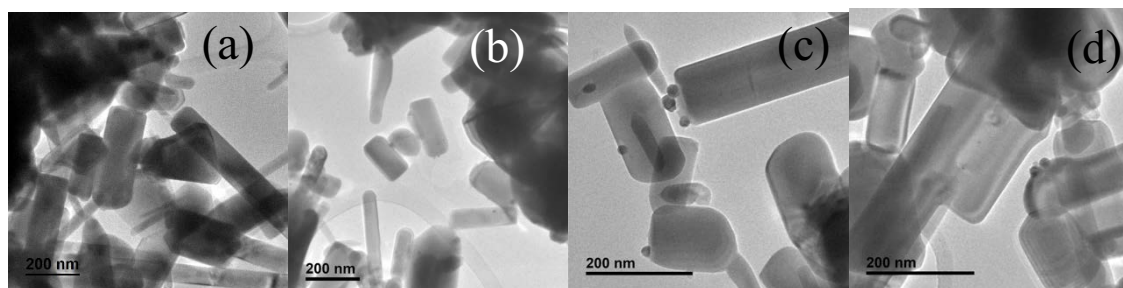
Fig. 3. TEM micrographs of ZnO (a), 1Ag/ZnO (b), 2Ag/ZnO (c) and 3Ag/ZnO (d).

The corresponding micrographs of the samples are included in Fig. 3. The TEM micrographs revealed that the ZnO were nanorods, and the particle sizes were varied. Cylindrical and quasi-spherical shapes were observed after the incorporation of silver in ZnO. Moreover, Ag nanoparticles were not found in our TEM observations, which indicated that all metallic Ag nanoparticles are dispersed in ZnO nanorods. The diameter of the Ag nanoparticles was 15, 20 and 30 nm for 1Ag/ZnO, 2Ag/ZnO and 3Ag/ZnO, respectively.

The surface morphology of the 2Ag/ZnO catalyst was analyzed by high-resolution transmission electron microscopy (HR-TEM); the images are shown in Fig. 4. The image revealed a distinguishable interface and the continuity of lattice fringes between the ZnO nanorods and the metallic Ag nanoparticles, which confirmed the formation of a chemical bond between them. In Fig. 4, the image also shows the uniform lattice structure and the single-crystalline nature of the ZnO nanorod. The spacing between adjacent lattice fringes was 2.6 Å, which is close to the d spacing of the (002) plane of ZnO [24]. In contrast, the Ag nanoparticle showed lattice fringes at the interplanar spacing of 2.4 Å, which corresponded to the (111) planes of the face-centered cubic

phase of metallic Ag [22,24]. The fast Fourier transform pattern also confirmed that FCC metallic Ag along the (002) plane was 2.04 Å (Fig. 4) [22]. The HR-TEM results agreed with the XRD (Fig. 2).

The DRS of ZnO, 1Ag/ZnO, 2Ag/ZnO, and 3Ag/ZnO are shown in Fig. 5a. The Ag^0 nanoparticles might have interacted covalently interact with ZnO, thus reducing its bandgap. Metal doping produced some energy levels between the valence band and conduction band in ZnO. Therefore, the Ag containing ZnO photocatalysts can be ascribed to the charge transfer between the valence or conduction band and the energy levels formed by silver [37]. In addition, UV-vis spectra in the diffuse reflectance mode were transformed to the Kubelka-Munk function to determine the bandgap energy (E_g) in the photocatalysts (Fig. 5b) [28]. The E_g values for ZnO, 1Ag/ZnO, 2Ag/ZnO, and 3Ag/ZnO were 3.20, 3.17, 3.18 and 3.19 eV, respectively, which were lower than the 3.20 eV value of ZnO. The observed bandgap of ZnO decreased as the silver concentration increased from 1% to 3%. These results confirmed than the xAg/ZnO catalysts were active in the UV region [38].

To determine the surface components and oxidation states of the Ag, Zn and O present in this photocatalysis, the
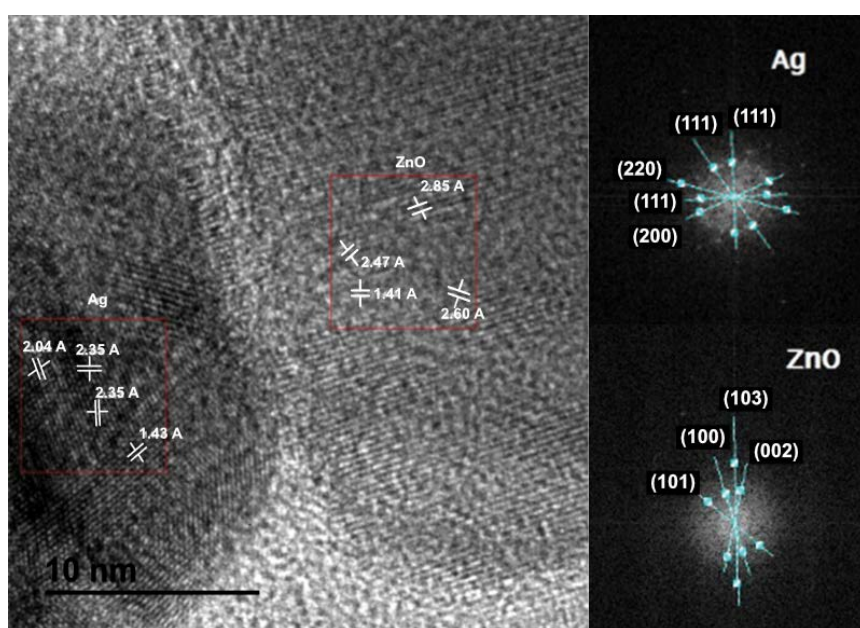
Fig. 4. HR-TEM micrograph of 2Ag/ZnO catalyst.
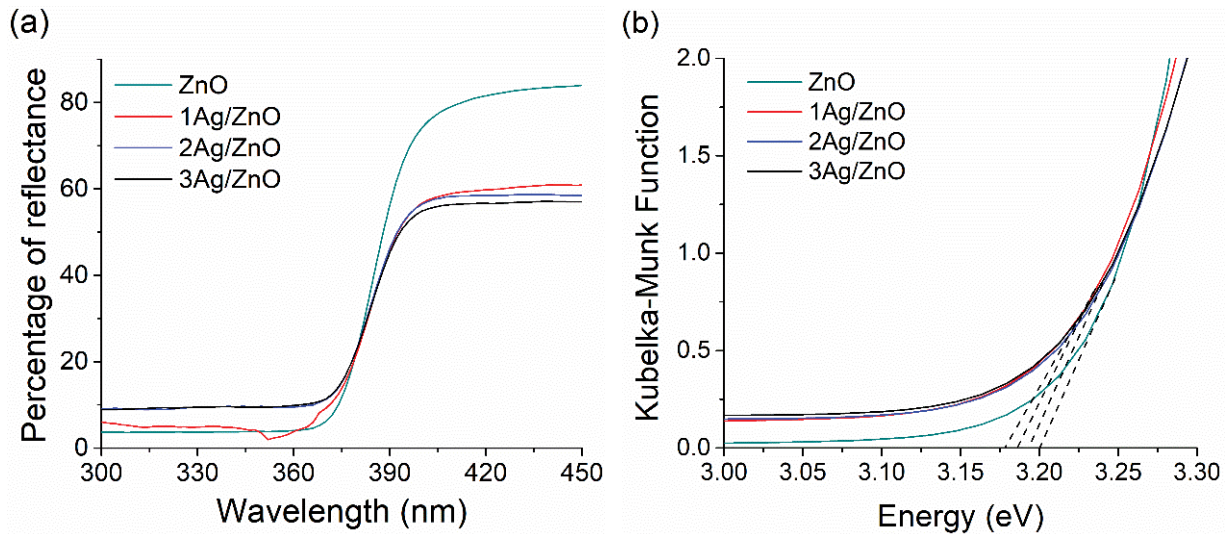
Fig. 5. Diffuse reflectance spectra (a) and plot of transferred Kubelka-Munk vs. energy (b) of the light absorbed of the catalysts.
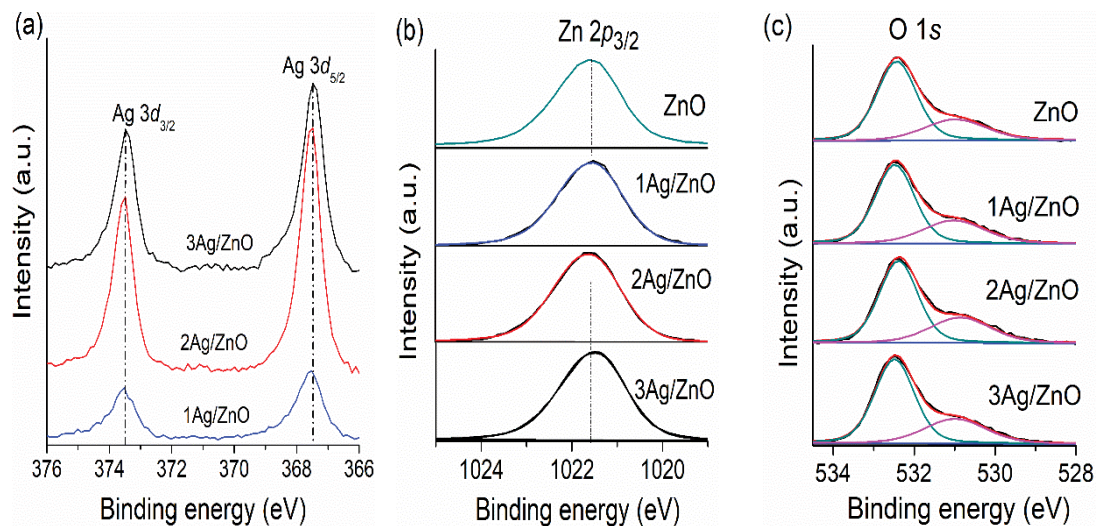
Fig. 6. XPS spectra of Ag 3d, Zn 2p and O 1s signals for ZnO, 1Ag/ZnO, 2Ag/ZnO and 3Ag/ZnO.

XPS of these samples was registered. The binding energy values of Ag 3d, Zn 2p and O 1s are presented in Fig. 6. The Ag 3d core-level spectra with doublet Ag $3d_{3/2}$ and Ag $3d_{5/2}$ at 373.5 and 367.5 eV, respectively, were attributed to silver metallic (Ag^0) [25,39,40], which was supported by the XRD patterns and HR-TEM. In all catalysts, the Zn $2p_{3/2}$ binding energy value was 1,021.6 eV, indicating an oxidation state of Zn^{2+} in the form of ZnO (Fig. 6b) [21,24]. Fig. 6c shows that the decomposition of the O 1s core-level spectra was split into two contributions at 530.1 eV, which was attributed to the lattice oxygen of ZnO [41], whereas the contribution at 531.8 eV was to the surface OH groups [21,25]. The area of 2Ag/ZnO catalyst was greater than the areas of 1Ag/ZnO and 3Ag/ZnO, indicating that the 2Ag/ZnO sample possessed a greater number of OH groups on the surface. Remarkably, the surface hydroxyls generate primary active $^{\bullet}$OH radicals, which are highly significant for photocatalyst [23].

FTIR spectra of 1Ag/ZnO, 2Ag/ZnO and 3Ag/ZnO are shown in Fig. 7. The spectra are similar in all samples. The absorption band peak at 436 cm^{-1} was attributed to Zn–O stretching [42]. The peak observed at 3,385 cm^{-1} corresponded to the stretching vibration of the O–H bond. These stretching vibrations indicated the presence of water molecules on the surface of the samples [38].

3.2. Catalytic activity

The results of the degradation of MB and MO under UV irradiation with the catalysts at 25°C are presented in Fig. 8. Fig. 8a shows the photocatalytic results for the degradation of MO; Fig. 8b shows those related to MB. The experiments performed without catalyst and with illumination showed no dye degradation, which indicated that the catalyst was essential for rapid photodegradation. Pure ZnO showed lower photocatalytic activity than the
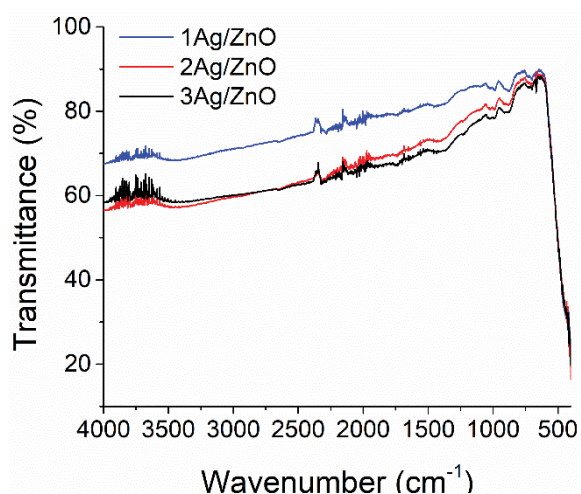
Fig. 7. Fourier-transform infrared spectra of 1Ag/ZnO, 2Ag/ZnO and 3Ag/ZnO.

xAg/ZnO samples did, which was likely due to the rapid recombination of photogenerated electrons-holes pairs [23,24]. The higher photocatalytic activity of the xAg/ZnO catalysts could be associated with metallic silver, which acted as an electron trap and inhibited e⁻–h⁺ recombination [18,22,25,36]. The best performance was achieved by the 2Ag/ZnO catalyst, which required 30 and 90 min to photodegrade MB and MO, respectively. The degradation of MO and MB in 2Ag/ZnO was a function of many physical and chemical parameters, including BET surface area, silver nanoparticles dispersion on ZnO and higher amounts of surface OH groups (Fig. 6c). The order of photocatalytic activity by the catalyst was as follows: 2Ag/ZnO > 3Ag/ZnO > 1Ag/ZnO > ZnO. The differences in the degradation of both dyes were due to the anionic (MO) and cationic (MB) natures of the molecules. MO reacted with cationic elements of the catalyst, whereas MB interacted with Columbic forces with the anionic elements (OH groups) [43]. The result that

MB degraded more rapidly than MO indicated the presence of a large population of surface hydroxyl groups (Fig. 6c).

The degradation of MB and MO was deemed a pseudo-first-order reaction. The photocatalytic process was expressed as follows $\ln(C_0/C_t) = kt + A$, where t is irradiation time and k is a pseudo-first-rate kinetic constant [44]. The kinetics of the catalysts in the photodegradation of the dyes are presented in Fig. 9. The k value was decided by linear fitting for various catalysts. The k values for MO were 0.017, 0.030, 0.050 and 0.035 min⁻¹ in ZnO, 1Ag/ZnO, 2Ag/ZnO and 3Ag/ZnO, respectively. The rate constants for MB were 0.023, 0.096, 0.184 and 0.114 min⁻¹ in ZnO, 1Ag/ZnO, 2Ag/ZnO and 3Ag/ZnO, respectively. The results showed that the k values of all Ag/ZnO samples were higher than those of ZnO. The 2Ag/ZnO catalyst exhibited the largest photocatalytic performance in MB and MO.

3.2.1. Detection of hydroxyl and superoxide radicals and the study of positive holes

In the mechanism of photocatalytic degradation, the 2Ag/ZnO catalyst was the most active, so it was selected to observe the following (1) the possible formation of •OH radicals; (2) the role of $O_2^{\bullet-}$ radicals based on bubbled nitrogen in the reaction; (3) the influence of the positive hole (h⁺) in the photocatalytic process by $(NH_4)_2C_2O_4$ as the hole collector.

The possible production of •OH radicals was evaluated by fluorescence spectroscopy using coumarin to capture them and form 7-hydroxycoumarin. This compound exhibited a characteristic emission band between 400 and 600 nm, as shown in Fig. 10. The intensity of the signal due to the 7-hydroxycoumarin compound was lower in the 2Ag/ZnO catalyst, which implies that the amount of •OH radicals was lower than that in ZnO. Therefore, the addition of silver decreased the capability of producing •OH radicals.

The presence of $O_2^{\bullet-}$ radicals during degradation was elucidated by studying the photodegradation of MB and MO with 2Ag/ZnO at 25°C in nitrogen and oxygen. Fig. 11 shows the UV-visible spectra at different reaction times.
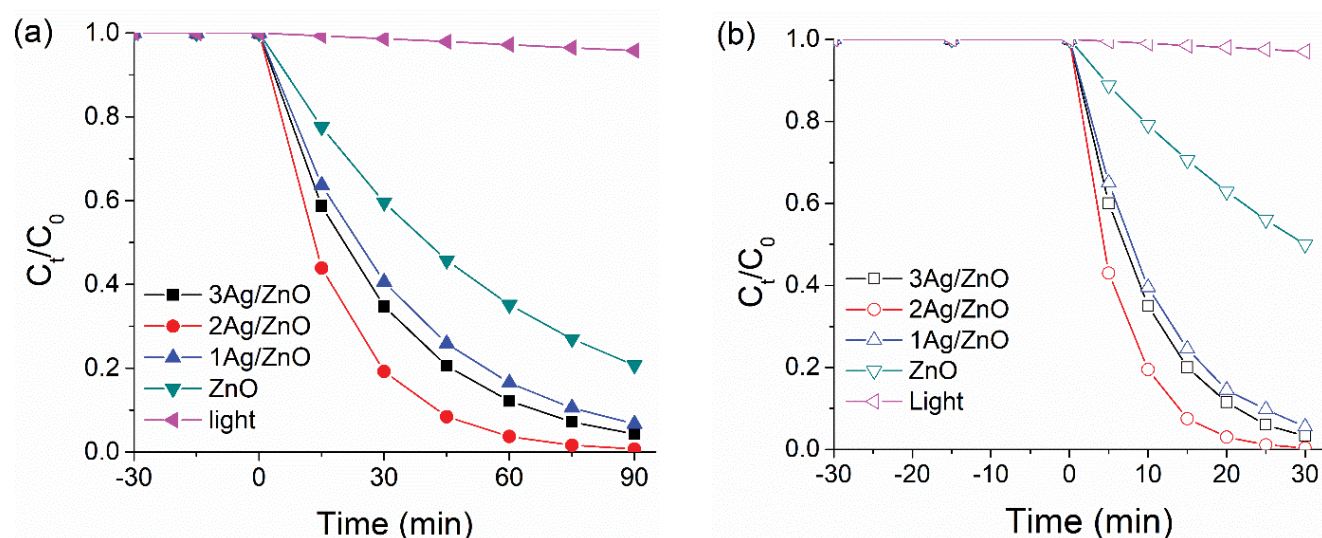
Fig. 8. Photodegradation of (a) MO and (b) MB in the absence and with catalysts under UV irradiation at 90 and 30 min.
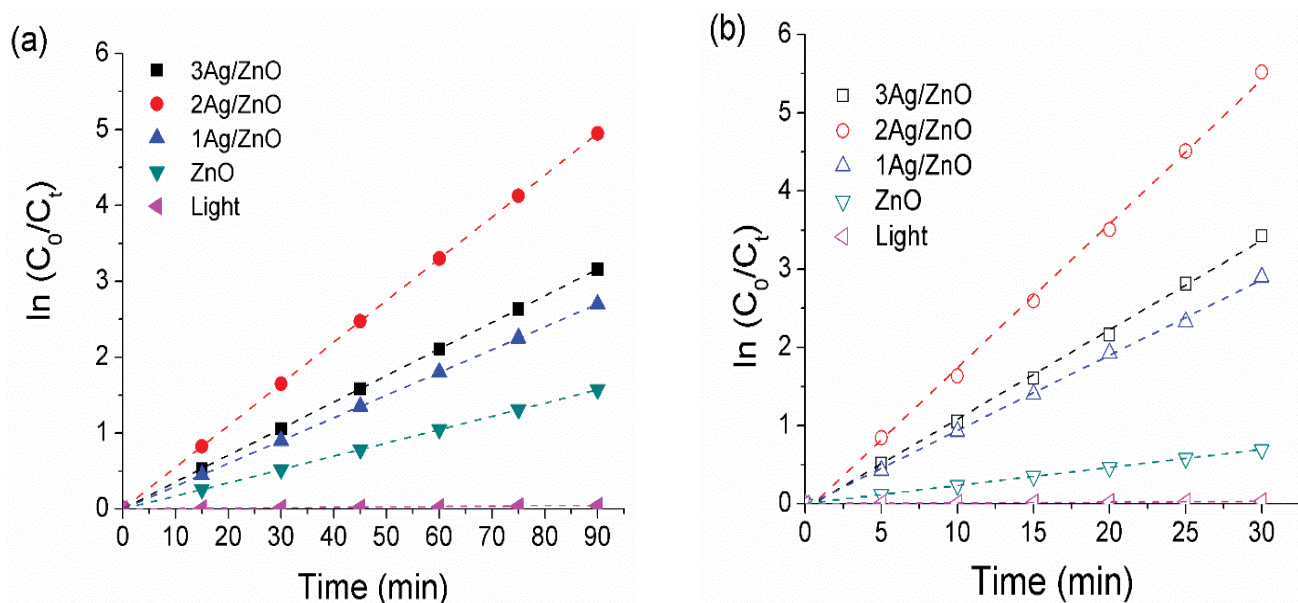
Fig. 9. The plot of $\ln(C_0/C_t)$ vs. time (a) MO and (b) MB in the absence and with a catalyst at 25°C.
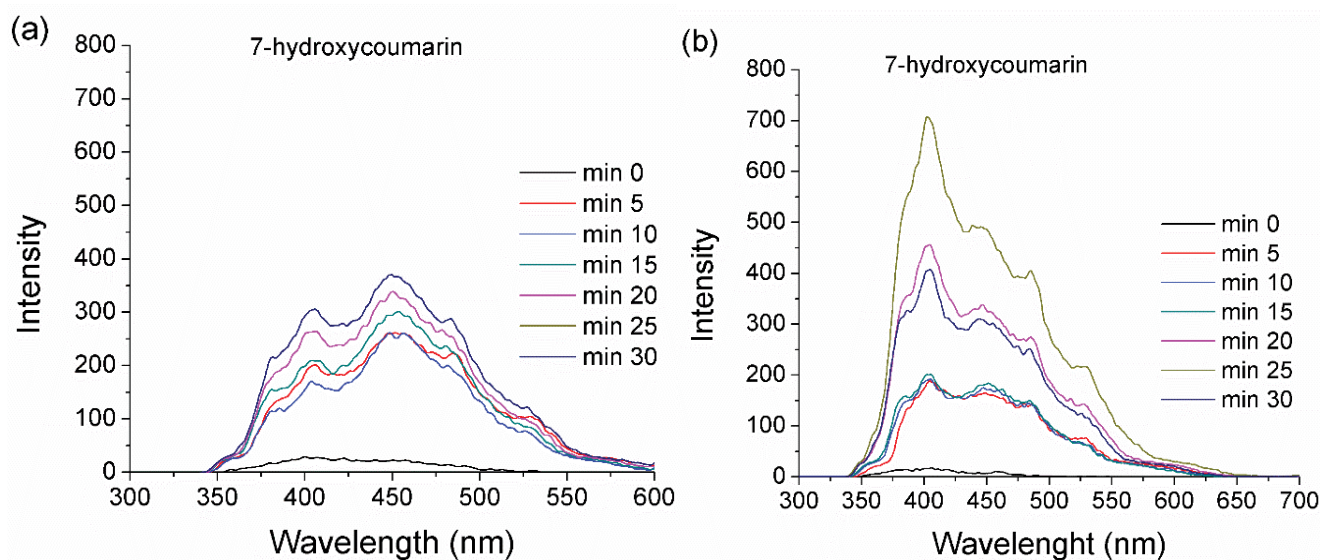
Fig. 10. Fluorescence spectra of 7-hydroxycoumarin employed to detect $^{\bullet}$OH radical formation for 2Ag/ZnO (a) and ZnO (b) samples at 25°C.

The UV-visible spectra corresponding to MB photodegradation in an oxygen atmosphere (Fig. 12a) showed four absorption peaks at 664, 612, 292 and 246 nm, the intensity of which decreased with reaction time. These bands corresponded to the UV-vis absorption of the monomers (612 and 664 nm) and oligomers (dimers and trimers at 246 and 292 nm) of MB in aqueous solutions. The latter was related to substituted benzenes rings [45]. The spectra did not show the appearance of new peaks, thus indicating the decomposition of MB during the process. The sharp decrease in absorbance intensity after 15 min confirmed that the MB monomers, dimers and trimers were broken rapidly [45].

The test carried out in a N_2 atmosphere, the spectra showed that the same absorption peaks corresponded to the MB signals, but their disappearance occurred much more slowly. In MO tests showed that the spectra exhibited two main absorption bands at 463 and 272 nm, which were due to the dye. Similar observations were made in comparison with MB degradation, which, however, was much faster in an oxygen atmosphere, and no additional peaks were observed.

The partial degradation of MB and MO in the absence of oxygen suggested the participation of the photogenerated hole (h^+) in the catalyst. However, the generation of $O_2^{\bullet-}$ radicals was responsible for the degradation of both dyes.
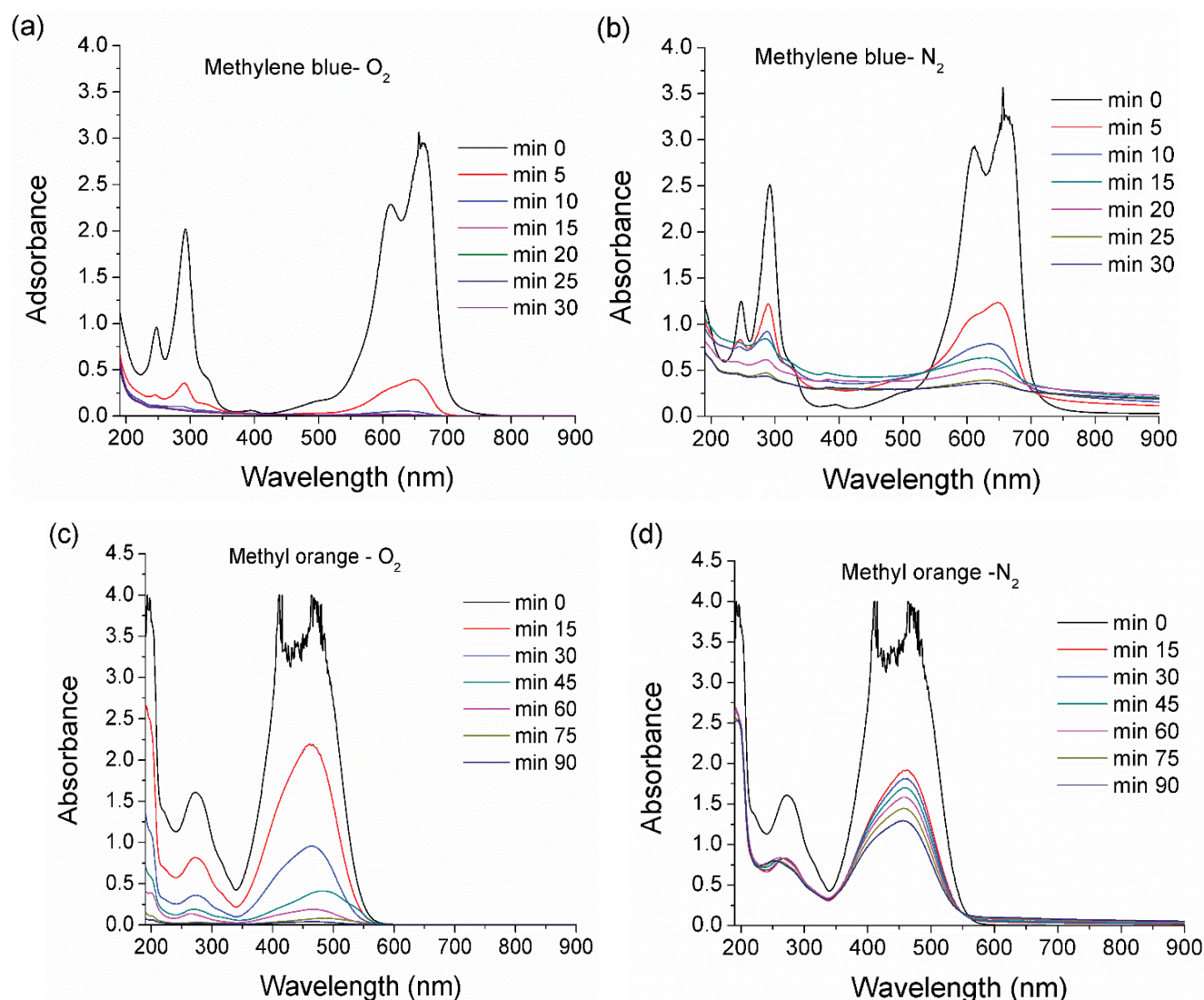
Fig. 11. UV-visible spectra of methylene blue and methyl orange degradation with 2Ag/ZnO catalyst in the presence of oxygen or nitrogen at 25°C.

To corroborate the role of the positive hole (h$^+$) in the degradation mechanism, a test was performed using ammonium oxalate as the hole scavenger to capture the photogenerated holes. In Fig. 12, the UV-visible absorption spectra corresponded to the photodegradation of MB and MO with 2Ag/ZnO in oxygen and under nitrogen flow. As previously observed in the MB spectra, only the dye absorption bands appeared, and the photodegradation was greater in the presence of oxygen, however, was slower when ammonium oxalate was present. These results indicated that the degradation of MB in the 2Ag/ZnO sample depended on the presence of superoxide radicals, as well as the presence of hydroxyl groups on the surface.

For MO, the degradation degree was slower when ammonium oxalate was present in the oxygen atmosphere but faster under nitrogen flow. These results indicated that positive holes did not play a dominant role in the photodegradation of MO under UV irradiation, which was similarly reported by Chen et al. [46]. Hence, the superoxide radical is the main reactive species during the photocatalytic degradation of MB and MO.

Fig. 13 shows the proposed mechanism for the degradation of MB and MO based on the properties of the 2Ag/ZnO catalyst at 25°C and the different types of $^\bullet$OH and $O_2^{\bullet-}$ radicals and holes. The degradation of the MB and MO was due to the generation of $O_2^{\bullet-}$ radicals.

3.2.2. Determination of nitrate and sulfate ions

The concentrations of NO_3^- observed in the photodegradation products for MB at 30 min were 6.4, 11.7 and 8.4 ppm in 1Ag/ZnO, 2Ag/ZnO and 3Ag/ZnO, respectively. The concentrations of SO_4^{2-} were 3.0, 5.1 and 4.3 ppm in 1Ag/ZnO, 2Ag/ZnO and 3Ag/ZnO, respectively. In the case of MO photodegradation at 90 min, the NO_3^- concentrations were 7.5, 11.5 and 5.7 ppm in 1Ag/ZnO, 2Ag/ZnO and 3Ag/ZnO,
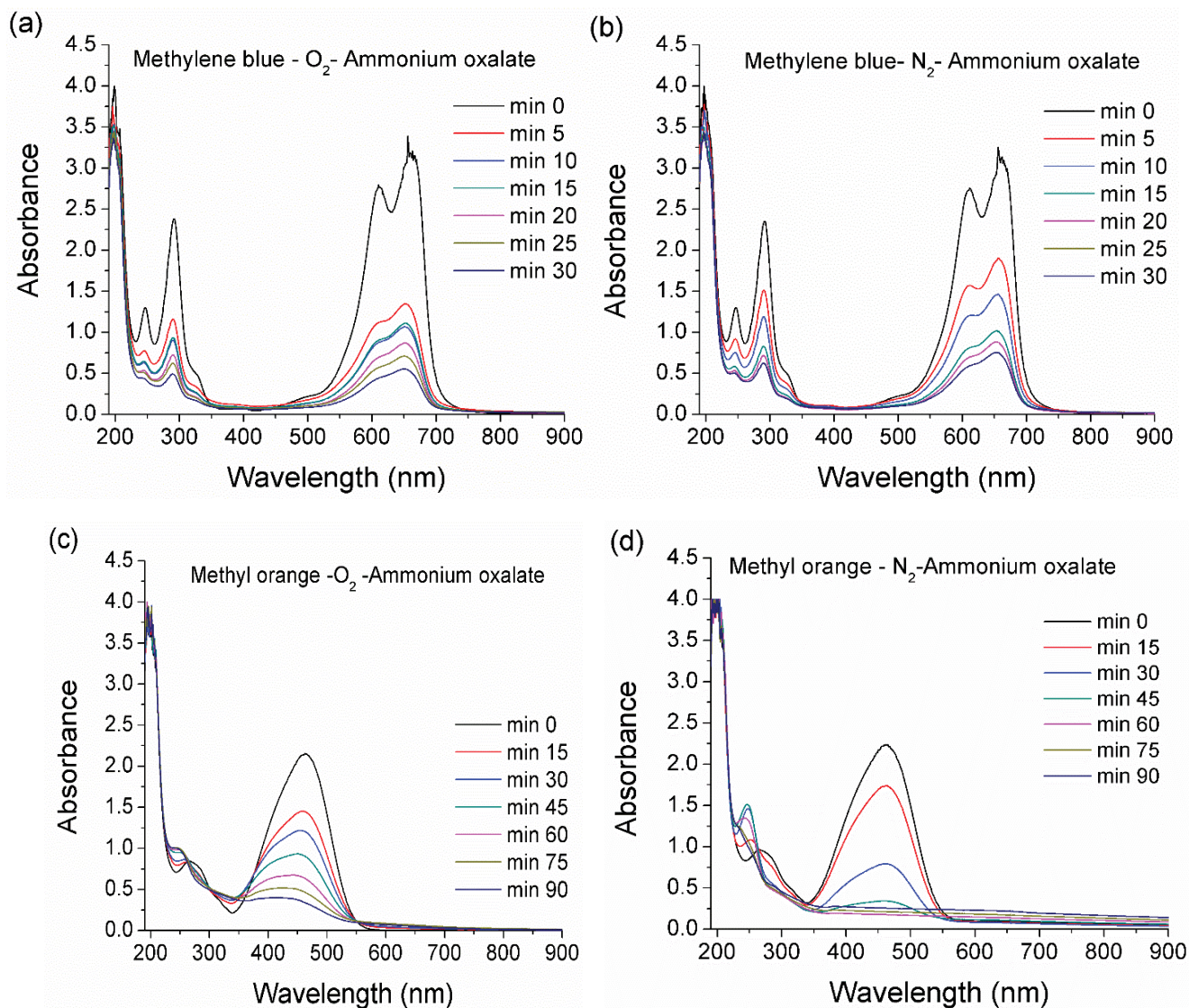
Fig. 12. UV-Vis spectra in the photodegradation of methylene blue and methyl orange in 2Ag/ZnO in the presence of ammonium oxalate with oxygen atmosphere or nitrogen flow.

respectively. The concentrations of SO_4^{2-} were 11.1, 22.6 and 19.1 ppm for 1Ag/ZnO, 2Ag/ZnO and 3Ag/ZnO, respectively. These results indicated that in both dyes, the most active catalyst was 2Ag/ZnO, which produced higher concentrations of nitrate and sulfate ions.

The FTIR spectra of 1Ag/ZnO, 2Ag/ZnO and 3Ag/ZnO catalysts after photodegradation reaction are shown in Fig. 14. The band at 3,385 cm^{-1} of O–H bond is observed after the reaction, and the new bands appear at 1,605; 1,352 and 1,117 cm^{-1} represented the C=O stretching mode, COH and CH, respectively, [38]. These compounds may have been due to the decomposition of dye molecule.

Fig. 15 shows the XRD patterns of the 1Ag/ZnO, 2Ag/ZnO and 3Ag/ZnO catalysts after photodegradation reaction. The presence of metallic silver on the surface of catalysts after the reactions and all the signals of the ZnO was observed, indicating that the catalysts exhibited excellent stability.

To understand the stability of the photocatalytic activity of 2Ag/ZnO is used to photodegrade MB and MO at 30 and 90 min five repeated cycles (Fig. 16). After five cycles, the 2Ag/ZnO sample exhibited remarkable photocatalytic stability, clearly demonstrating that the 2Ag/ZnO catalyst present favorable photostability under UV irradiation.

The application of heterogeneous catalysis to degrade dye molecules present in water is of great interest. Table 2 presents the results in the literature regarding dye degradation using Ag/ZnO catalysts for comparison with the 2Ag/ZnO catalyst presented here, which showed increased photocatalytic activity.

The degradation of MO and MB in 2Ag/ZnO were a function of many physical and chemical parameters, including BET surface area, silver nanoparticles dispersion on ZnO and higher amounts of surface OH groups. Moreover, the degradation of MB and MO was due to the formation of $O_2^{\bullet-}$
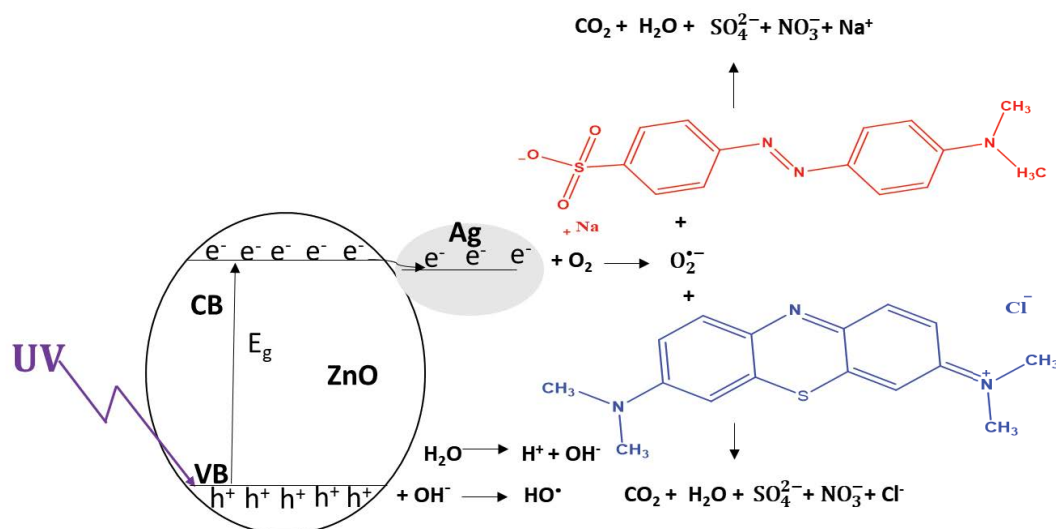
Fig. 13. A possible route for the degradation of MB and MO in 2Ag/ZnO at 25°C.
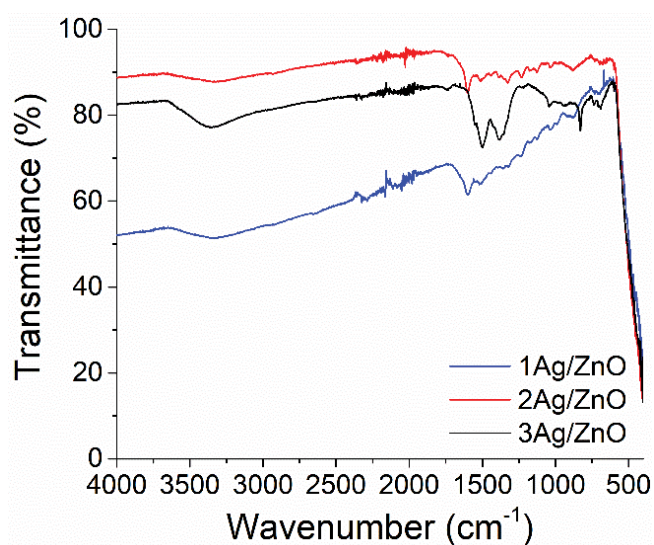
Fig. 14. Fourier-transform infrared spectra of 1Ag/ZnO, 2Ag/ZnO and 3Ag/ZnO.
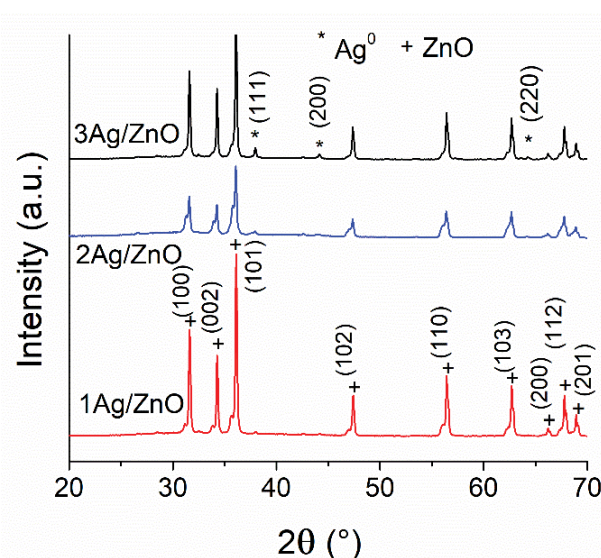
Fig. 15. XRD patterns of 1Ag/ZnO, 2Ag/ZnO and 3Ag/ZnO after photodegradation reaction.

radicals. The 2Ag/ZnO catalyst exhibited excellent photocatalytic stability and activity after five cycles.

4. Conclusion

This work reported the preparation and characterization of silver on zinc oxide catalysts for the photodegradation of MB and MO. The Ag^0 was supported on ZnO, which was confirmed by XRD, HR-TEM and XPS. Photocatalytic degradation showed that the incorporation of Ag^0 nanoparticles to ZnO resulted in faster rates of degradation of both dyes compared with ZnO alone. The 2Ag/ZnO catalysts showed 100% degradation of MB and MO at 30 and 90 min, respectively, which was due to its greater dispersion of the silver nanoparticles on ZnO and the presence of higher concentrations of surface OH groups compared with the

other catalysts. Moreover, 2Ag/ZnO catalyst exhibited excellent photocatalytic stability and activity after five cycles. Based on the results of the present study, the degradation mechanism proposed for the photodegradation of methylene blue (MB) and MO blue is the formation of $O_2^{\bullet-}$ radicals.

Table 2
Summary of recent research reports pertaining to the synthesis of ZnO with Ag and their application as photocatalysts

Sr. No.	Photocatalyst material	Dye solution tested	Catalyst quantity	Light source used	Remarks	References
1	Ag-doped ZnO nanospindles	5 mL of 3 ppm MO solution	5 mg	Sunlight	100% degradation in 60 min	[22]
2	Ag-doped ZnO microspheres	250 mL of 30 ppm MB solution	125 mg	Xenon lamp (450 W and 400 nm)	93% degradation in 180 min	[23]
3	Ag–ZnO nanocomposite	10 ppm of MB and MO solution	Not mentioned	l > 500 nm	85% and 77% for MB and MO at 4 and 5 h	[24]
4	Ag–ZnO nanorods	20 mL of 5 ppm MO solution	Not mentioned	Xenon light (300 W and 400 nm)	90% degradation MO at 120 min	[25]
5	ZnO/Ag nanocomposites	500 mL of 16 ppm of MB and MO	Not mentioned	250 W (l > 532 nm)	Complete degradation of MB and MO at 120 min	[21]
6	Ag–ZnO multiponds	100 mL of 10 and 5 ppm of MO and MB solution	40 mg	400 W	100% degradation of MO and MB in 60 min	[36]
7	Ag supported on ZnO	450 mL of 20 ppm MB and MO solution	150 mg	Mercury lamp (400 W)	Complete degradation for MB and MO in 30 and 90 min	Present work
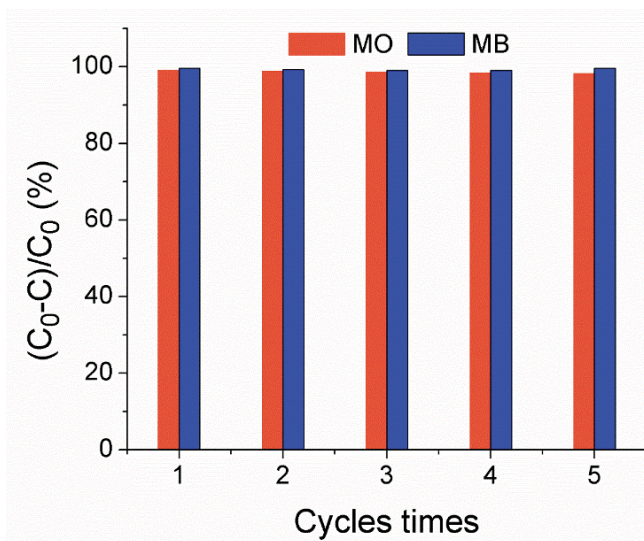
Fig. 16. Percentage of degradation of MB and MO in 2Ag/ZnO at 30 and 90 min after 5 cycles.

References

[1] M. Rafatullah, O. Sulaiman, R. Hashim, A. Ahmad, Adsorption of methylene blue on low-cost adsorbents: a review, J. Hazard. Mater., 177 (2010) 70–80.

[2] N.F. Cardoso, E.C. Lima, B. Royer, M.V. Bach, G.L. Dotto, L.A.A. Pinto, T. Calvete, Comparison of *Spirulina platensis* microalgae and commercial activated carbon as adsorbents for the removal of Reactive Red 120 dye from aqueous effluents, J. Hazard. Mater., 241–242 (2012) 146–153.

[3] A. Kausar, M. Iqbal, A. Javed, K. Aftab, Zill-i-Huma Nazli, H.N. Bhatti, S. Nouren, Dyes adsorption using clay and modified clay: a review, J. Mol. Liq., 256 (2018) 395–407.

[4] A. Kandelbauer, G.M. Guebitz, Bioremediation for the Decolorization of Textile Dyes — A Review, E. Lichtfouse, J. Schwarzbauer, D. Robert, Eds., Environmental Chemistry: Green Chemistry and Pollutants in Ecosystems, Springer, Berlin, 2005, pp. 269–288.

[5] S.M. Al-Rashed, A.A. Al-Gaid, Kinetic and thermodynamic studies on the adsorption behavior of Rhodamine B dye on Duolite C-20 resin, J. Saudi Chem. Soc., 16 (2012) 209–215.

[6] V. Sarria, M. Deront, P. Péringer, C. Pulgarin, Degradation of a biorecalcitrant dye precursor present in industrial wastewaters by a new integrated iron(III) photoassisted–biological treatment, Appl. Catal., B, 40 (2003) 231–246.

[7] A. Nezamzadeh-Ejhieh, M. Khorsandi, Heterogeneous photo-decolorization of Eriochrome Black T using Ni/P zeolite catalyst, Desalination, 262 (2010) 79–85.

[8] B. Bethi, S.H. Sonawane, B.A. Bhanvase, S.P. Gumfekar, Nanomaterials-based advanced oxidation processes for wastewater treatment: a review, Chem. Eng. Process., 109 (2016) 178–189.

[9] C. Comninellis, A. Kapalka, S. Malato, S.A. Parsons, I. Poulios, D. Mantzavinos, Advanced oxidation processes for water treatment: advances and trends for R&D, J. Chem. Technol. Biotechnol., 83 (2008) 769–776.

[10] D. Kanakaraju, B.D. Glass, M. Oelgemöller, Advanced oxidation process-mediated removal of pharmaceuticals from water: a review, J. Environ. Manage., 219 (2018) 189–207.

[11] T.W. Chen, Y.H. Zheng, J.-M. Lin, G.N. Chen, Study on the photocatalytic degradation of methyl orange in water using Ag/ZnO as catalyst by liquid chromatography electrospray ionization ion-trap mass spectrometry, J. Am. Soc. Mass. Spectrom., 19 (2008) 997–1003.

[12] J.W. Fang, H.Q. Fan, G.Z. Dong, A facile way to synthesize cost-effective ZnO nanorods with enhanced photocatalytic activity, Mater. Lett., 120 (2014) 147–150.

[13] L.Q. Jiang, L. Gao, Fabrication and characterization of ZnO-coated multi-walled carbon nanotubes with enhanced photocatalytic activity, Mater. Chem. Phys., 91 (2005) 313–316.

[14] H. Anwar, B.C. Rana, Y. Javed, G. Mustafa, M.R. Ahmad, Y. Jamil, H. Akhtar, Effect of ZnO on photocatalytic degradation

of Rh B and its inhibition activity for *C. coli* bacteria, Russ. J. Appl. Chem., 91 (2018) 143–149.

[15] R.D. Suryavanshi, S.V. Mohite, A.A. Bagade, S.K. Shaikh, J.B. Thorat, K.Y. Rajpure, Nanocrystalline immobilised ZnO photocatalyst for degradation of benzoic acid and methyl blue dye, Mater. Res. Bull., 101 (2018) 324–333.

[16] R. Ahumada-Lazo, L.M. Torres-Martínez, M.A. Ruíz-Gómez, O.E. Vega-Becerra, M.Z. Figueroa-Torres, Photocatalytic efficiency of reusable ZnO thin films deposited by sputtering technique, Appl. Surf. Sci., 322 (2014) 35–40.

[17] S. Ghattavi, A. Nezamzadeh-Ejhieh, A brief study on the boosted photocatalytic activity of AgI/WO$_3$/ZnO in the degradation of Methylene Blue under visible light irradiation, Desal. Water Treat., 166 (2019) 92–104.

[18] Y.H. Zheng, L.R. Zheng, Y.Y. Zhan, X.Y. Lin, Q. Zheng, K. Wei, Ag/ZnO heterostructure nanocrystals: synthesis, characterization, and photocatalysis, Inorg. Chem., 46 (2007) 6980–6986.

[19] M.J. Height, S.E. Pratsinis, O. Mekasuwandumrong, P. Praserthdam, Ag–ZnO catalysts for UV-photodegradation of methylene blue, Appl. Catal., B, 63 (2006) 305–312.

[20] N. Chekir, O. Benhabiles, D. Tassalit, N.A. Laoufi, F. Bentahar, Photocatalytic degradation of methylene blue in aqueous suspensions using TiO$_2$ and ZnO, Desal. Water Treat., 57 (2016) 6141–6147.

[21] R. Saravanan, N. Karthikeyan, V.K. Gupta, E. Thirumal, P. Thangadurai, V. Narayanan, A. Stephen, ZnO/Ag nanocomposite: an efficient catalyst for degradation studies of textile effluents under visible light, Mater. Sci. Eng. C, 33 (2013) 2235–2244.

[22] S. Kuriakose, V. Choudhary, B. Satpati, S. Mohapatra, Facile synthesis of Ag–ZnO hybrid nanospindles for highly efficient photocatalytic degradation of methyl orange, Phys. Chem. Chem. Phys., 16 (2014) 17560–17568.

[23] X.D. Zhang, Y.X. Wang, F.L. Hou, H.X. Li, Y. Yang, X.X. Zhang, Y.Q. Yang, Y. Wang, Effects of Ag loading on structural and photocatalytic properties of flower-like ZnO microspheres, Appl. Surf. Sci., 391 (2017) 476–483.

[24] S.A. Ansari, M.M. Khan, M.O. Ansari, J. Lee, M.H. Cho, Biogenic synthesis, photocatalytic, and photoelectrochemical performance of Ag–ZnO nanocomposite, J. Phys. Chem. C, 117 (2013) 27023–27030.

[25] J. Lu, H.H. Wang, S.J. Dong, F.Q. Wang, Y.F. Dong, Effect of Ag shapes and surface compositions on the photocatalytic performance of Ag/ZnO nanorods, J. Alloys Compd., 617 (2014) 869–876.

[26] S. Brunauer, P.H. Emmett, E. Teller, Adsorption of gases in multimolecular layers, J. Am. Chem. Soc., 60 (1938) 309–319.

[27] S. Das, S. Kar, S. Chaudhuri, Optical properties of SnO$_2$ nanoparticles and nanorods synthesized by solvothermal process, J. Appl. Phys., 99 (2006) 114303.

[28] G. Kortüm, Reflectance Spectroscopy: Principles, Methods, Applications, Springer, Berlin, 1969.

[29] Z.-R. Lin, L. Zhao, Y.-H. Dong, Quantitative characterization of hydroxyl radical generation in a goethite-catalyzed Fenton-like reaction, Chemosphere, 141 (2015) 7–12.

[30] Y. Nosaka, A.Y. Nosaka, Generation and detection of reactive oxygen species in photocatalysis, Chem. Rev., 117 (2017) 11302–11336.

[31] E.M. Rodríguez, G. Márquez, M. Tena, P.M. Álvarez, F.J. Beltrán, Determination of main species involved in the first steps of TiO$_2$ photocatalytic degradation of organics with the use of scavengers: the case of ofloxacin, Appl. Catal., B, 178 (2015) 44–53.

[32] W. Liu, M.L. Wang, C.X. Xu, S.F. Chen, X.L. Fu, Significantly enhanced visible-light photocatalytic activity of g-C$_3$N$_4$ via ZnO modification and the mechanism study, J. Mol. Catal. A: Chem., 368–369 (2013) 9–15.

[33] E.W. Rice, R.B. Baird, A.D. Eaton, L.S. Clesceri, Standard Methods for the Examination of Water and Wastewater, 22nd ed., American Public Health Association, Washington, 2012.

[34] T. Dambrauskas, K. Baltakys, A. Eisinas, S. Kitrys, The specific surface area and porosity of synthetic and calcined α-C$_2$SH, kilchoanite and hydroxyledgrewite, Powder Technol., 355 (2019) 504–513.

[35] E.P. Barrett, L.G. Joyner, P.P. Halenda, The determination of pore volume and area distributions in porous substances. I. Computations from nitrogen isotherms, J. Am. Chem. Soc., 73 (1951) 373–380.

[36] M. Arab Chamjangali, G. Bagherian, A. Javid, S. Boroumand, N. Farzaneh, Synthesis of Ag–ZnO with multiple rods (multipods) morphology and its application in the simultaneous photo-catalytic degradation of methyl orange and methylene blue, Spectrochim. Acta, Part A, 150 (2015) 230–237.

[37] B. Subash, B. Krishnakumar, M. Swaminathan, M. Shanthi, Highly efficient, solar active, and reusable photocatalyst: Zr-loaded Ag–ZnO for Reactive Red 120 dye degradation with synergistic effect and dye-sensitized mechanism, Langmuir, 29 (2013) 939–949.

[38] M. Vinayagam, S. Ramachandran, V. Ramya, A. Sivasamy, Photocatalytic degradation of orange G dye using ZnO/biomass activated carbon nanocomposite, J. Environ. Chem. Eng., 6 (2018) 3726–3734.

[39] X.D. Zhang, Y. Yang, L. Song, Y.X. Wang, C. He, Z. Wang, L.F. Cui, High and stable catalytic activity of Ag/Fe$_2$O$_3$ catalysts derived from MOFs for CO oxidation, Mol. Catal., 447 (2018) 80–89.

[40] X.D. Zhang, Y. Yang, X.T. Lv, Y.X. Wang, L.F. Cui, Effects of preparation method on the structure and catalytic activity of Ag–Fe$_2$O$_3$ catalysts derived from MOFs, Catalysts, 7 (2017) 1–13.

[41] Y.Q. Yang, H. Dong, Y. Wang, C. He, Y.X. Wang, X.D. Zhang, Synthesis of octahedral like Cu-BTC derivatives derived from MOF calcined under different atmosphere for application in CO oxidation, J. Solid State Chem., 258 (2018) 582–587.

[42] M. Faisal, S.B. Khan, M.M. Rahman, A. Jamal, K. Akhtar, M.M. Abdullah, Role of ZnO-CeO$_2$ nanostructures as a photocatalyst and chemi-sensor, J. Mater. Sci. Technol., 27 (2011) 594–600.

[43] L.V. Trandafilović, D.J. Jovanović, X. Zhang, S. Ptasińska, M.D. Dramićanin, Enhanced photocatalytic degradation of methylene blue and methyl orange by ZnO:Eu nanoparticles, Appl. Catal., B, 203 (2017) 740–752.

[44] K.V. Kumar, K. Porkodi, F. Rocha, Langmuir–Hinshelwood kinetics – a theoretical study, Catal. Commun., 9 (2008) 82–84.

[45] S. Senobari, A. Nezamzadeh-Ejhieh, A comprehensive study on the photocatalytic activity of coupled copper oxide-cadmium sulfide nanoparticles, Spectrochim. Acta, Part A, 196 (2018) 334–343.

[46] X.Q. Chen, Z.S. Wu, D.D. Liu, Z.Z. Gao, Preparation of ZnO photocatalyst for the efficient and rapid photocatalytic degradation of azo dyes, Nanoscale Res. Lett., 12 (2017) 143.